Label-free quantitative proteomics of the lysine acetylome in mitochondria identifies substrates of SIRT3 in metabolic pathways

Matthew J. Rardin[a], John C. Newman[b,c], Jason M. Held[a], Michael P. Cusack[a], Dylan J. Sorensen[a], Biao Li[a], Birgit Schilling[a], Sean D. Mooney[a], C. Ronald Kahn[d,1], Eric Verdin[b,c], and Bradford W. Gibson[a,1]

[a]Buck Institute for Research on Aging, Novato, CA 94945; [b]Gladstone Institute of Virology and Immunology, San Francisco, CA 94158; [c]Department of Medicine, University of California, San Francisco, CA 94158; and [d]Department of Medicine, Joslin Diabetes Center, Harvard Medical School, Boston, MA 02215

Contributed by C. Ronald Kahn, February 21, 2013 (sent for review December 20, 2012)

Large-scale proteomic approaches have identified numerous mitochondrial acetylated proteins; however in most cases, their regulation by acetyltransferases and deacetylases remains unclear. Sirtuin 3 (SIRT3) is an NAD$^+$-dependent mitochondrial protein deacetylase that has been shown to regulate a limited number of enzymes in key metabolic pathways. Here, we use a rigorous label-free quantitative MS approach (called MS1 Filtering) to analyze changes in lysine acetylation from mouse liver mitochondria in the absence of SIRT3. Among 483 proteins, a total of 2,187 unique sites of lysine acetylation were identified after affinity enrichment. MS1 Filtering revealed that lysine acetylation of 283 sites in 136 proteins was significantly increased in the absence of SIRT3 (at least twofold). A subset of these sites was independently validated using selected reaction monitoring MS. These data show that SIRT3 regulates acetylation on multiple proteins, often at multiple sites, across several metabolic pathways including fatty acid oxidation, ketogenesis, amino acid catabolism, and the urea and tricarboxylic acid cycles, as well as mitochondrial regulatory proteins. The widespread modification of key metabolic pathways greatly expands the number of known substrates and sites that are targeted by SIRT3 and establishes SIRT3 as a global regulator of mitochondrial protein acetylation with the capability of coordinating cellular responses to nutrient status and energy homeostasis.

Lysine acetylation is one of the most common posttranslational modifications among cellular proteins and regulates a variety of physiological processes including enzyme activity, protein–protein interactions, gene expression, and subcellular localization (1). Large-scale proteomic surveys have demonstrated that lysine acetylation is prevalent within mitochondria (2, 3). As the central regulators of cellular energy production, mitochondria require a coordinated response to changes in nutrient availability to respond to metabolic needs. In addition to ATP production, mitochondria are essential for regulation of fatty acid oxidation, apoptosis, and amino acid catabolism. Disruption of these processes is associated with a variety of neurodegenerative disorders and metabolic diseases (4, 5). Understanding the role of lysine acetylation in mitochondrial function will likely provide insight into altered metabolism in dysregulated or disease states.

The sirtuins (SIRT1–7) are an evolutionary conserved family of NAD$^+$-dependent deacetylases (6). SIRT3, SIRT4, and SIRT5 are major, if not exclusively, localized in the mitochondrial matrix (7, 8). SIRT3 is the primary regulator of mitochondrial lysine acetylation (9), whereas SIRT5 regulates lysine malonylation and succinylation (10, 11), and SIRT4 has no well established target except weak ADP ribosyltransferase activity (12). SIRT3 is highly expressed in mitochondria-rich tissues and shows differentially regulated expression in liver and skeletal muscle in response to changes in nutrient availability such as fasting, high-fat diet, and caloric restriction (13–15), suggesting a role in coordinating metabolic responses across these tissues. No mitochondrial acetyltransferase is known to date, and mitochondrial acetylation may be caused by a reaction of lysine residues with acetyl-CoA in a nonenzymatic process.

SIRT3 regulates the acetylation and enzymatic activity of key enzymes in several metabolic pathways. Hyperacetylation of complex I and complex II in the respiratory chain of SIRT3$^{-/-}$ (KO) mice leads to reduced activity, indicating a role for SIRT3 in regulation of oxidative phosphorylation machinery and ATP production (16–18). SIRT3 also regulates ketogenesis through activation of hydroxymethylglutaryl-CoA synthase 2 (HMGCS2) in the fasted state (19). KO mice show liver steatosis due to defective fatty acid oxidation through long-chain acyl-CoA dehydrogenase (ACADL) (14), and impaired insulin signaling in skeletal muscle due to increased oxidative stress (15). In addition, SIRT3 directly regulates oxidative stress through deacetylation and activation of superoxide dismutase (SOD2) (20–22). Lack of SIRT3 leads to a pseudohypoxic response associated with induction of hypoxia-inducible factor 1α stabilization and the Warburg effect, consistent with its tumor suppressor activity (23, 24). Finally, increased expression of SIRT3 during caloric restriction protects mice from age-related hearing loss through activation of isocitrate dehydrognease (IDH2) (25).

Recent reports have described widespread hyperacetylation of mitochondrial proteins in KO mice (9, 14, 15); however, the protein substrates and specific lysine residues that are deacetylated by SIRT3 remain largely unknown. To investigate the regulation of lysine acetylation in mitochondria and identify SIRT3 substrates, we used a quantitative proteomic approach to compare lysine acetylation in the fasted state in the liver of SIRT3$^{-/-}$ mice and WT animals. We demonstrate a robust method for enrichment of lysine acetylated peptides from liver mitochondria. Using a unique label-free quantitation method termed MS1 Filtering (26) in combination with a SIRT3$^{-/-}$ mouse model, we show that lysine acetylation increases in the absence of SIRT3 across a wide variety of mitochondrial proteins of critical importance to mitochondrial biology and metabolism.

Results

Enrichment and Identification of Lysine Acetylation Sites in Liver Mitochondria. To determine changes in the lysine acetylome in the absence of SIRT3, we developed a robust workflow for the

Author contributions: M.J.R., C.R.K., E.V., and B.W.G. designed research; M.J.R. performed research; M.J.R., J.C.N., J.M.H., M.P.C., D.J.S., B.L., B.S., and S.D.M. analyzed data; and M.J.R., C.R.K., E.V., and B.W.G. wrote the paper.

The authors declare no conflict of interest.

Freely available online through the PNAS open access option.

Data deposition: The raw mass spectrometry data files have been deposited using an FTP site hosted at the Buck Institute, ftp://sftp.buckinstitute.org/Gibson.

[1]To whom correspondence may be addressed. E-mail: c.ronald.kahn@joslin.harvard.edu or bgibson@buckinstitute.org.

This article contains supporting information online at www.pnas.org/lookup/suppl/doi:10.1073/pnas.1302961110/-/DCSupplemental.

identification and quantitation of acetylated lysine (acK) peptides (Fig. 1). Mice were fasted 24 h before tissue harvest to maximize SIRT3 expression in the WT (14). Liver mitochondria were isolated from five WT and five KO mice by differential centrifugation. Samples were normalized to total mitochondrial and Western analysis using mitochondrial markers confirmed equal amounts of mitochondrial enrichment across animals (Fig. 2*A*). To control for process variability, two mitochondrial fractions per animal were prepared in parallel for MS analysis. Each sample was digested with trypsin, and 100 fmol of a synthetic heavy labeled acK peptide was spiked-in for normalization (27). Peptides containing acK were immunoprecipitated using a combination of two polyclonal anti-acetyllysine antibodies because we found this increases the diversity and efficiency of acK peptides detected (26). The enriched acK peptides were analyzed in duplicate by LC-MS/MS on a TripleTOF 5600 mass spectrometer, and data were searched against the mouse proteome.

Using a false discovery rate (FDR) cutoff of ≤1%, we identified 2,806 unique acK peptides (Dataset S1) encompassing 2,187 unique acK sites across 483 proteins (Dataset S2), with an overlap of 69% and 66%, respectively, between WT and KO (Fig. 2*B*). A higher number of unique sites were identified in KO vs. WT mice (384 vs. 302). The majority of proteins were multiacetylated, with 61% having two or more acK sites (Fig. 2*C*). The most acetylated protein was the highly abundant urea cycle protein carbamoyl phosphate synthase (CPS1) with 70 of 97 lysines acetylated.

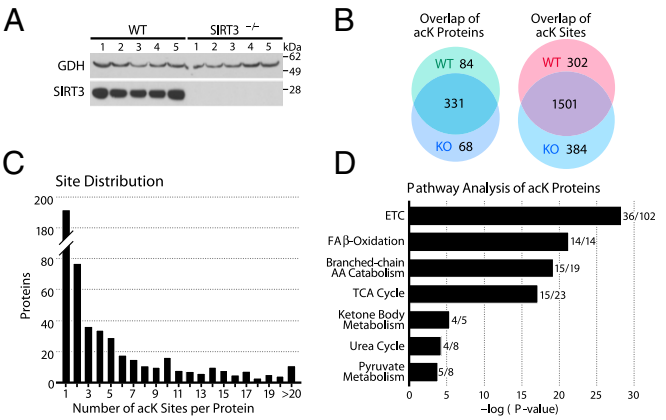

Fig. 2. Identification of acetylated peptides and proteins by LC-MS/MS. (*A*) Western blot analysis of glutamate dehydrogenase (GDH) and SIRT3 in mitochondrial lysates from WT and SIRT3$^{-/-}$ mouse livers. (*B*) Overlap of identified acetylated proteins and peptides from WT and SIRT3$^{-/-}$ mice. (*C*) Distribution of acK sites identified per protein. (*D*) Pathway analysis of the mitochondrial acetylome with the number of proteins identified per pathway indicated.

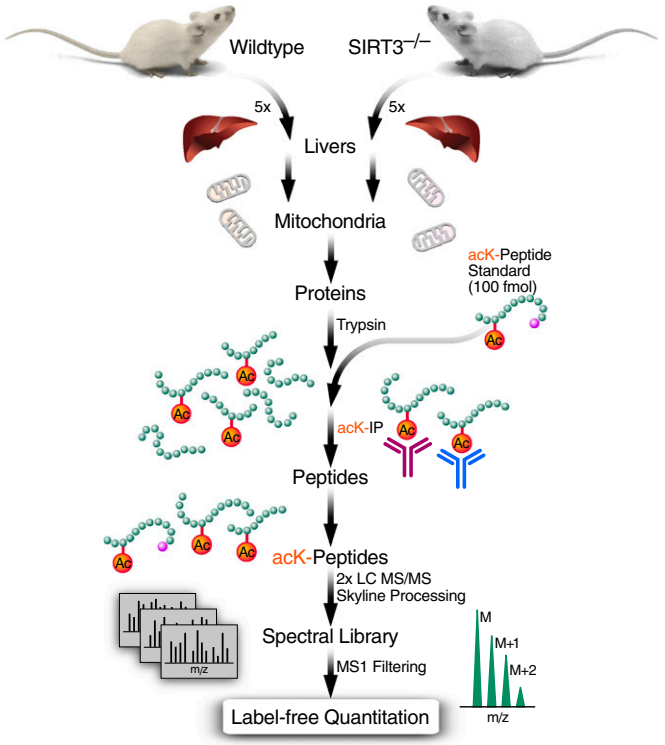

Fig. 1. Strategy for identification and quantitation of the SIRT3-regulated acetylome in mouse liver mitochondria. Liver mitochondria were isolated from five individual WT and SIRT3$^{-/-}$ male mice. Two process replicates from each of 10 mitochondrial protein isolates were digested separately with trypsin, generating 20 samples. The resulting peptide fractions were desalted, and 100 fmol of a heavy isotope-labeled acK-peptide standard (*m/z* 626.8604^{++}; LVSSVSDLPacK**R**-$^{13}C_6{}^{15}N_4$) was added. acK peptides were immunoprecipitated using two anti-acK antibodies. Enriched peptides were separated and analyzed in duplicate by HPLC-MS/MS. Data were processed using Skyline to generate a MS/MS spectral library of the identified acK peptides. Precursor ion intensity chromatograms for one or more isotopes (M, M+1, M+2) of each peptide were integrated using Skyline MS1 Filtering and used for label-free quantitation across all samples after normalization to the peak area of the peptide standard.

To determine whether a particular subset of the mitochondrial proteome was preferentially acetylated, we performed a pathway enrichment analysis of all acetylated proteins (28) (Fig. 2*D*). Notably, all proteins from the fatty acid oxidation (FAO) pathway were acetylated. In addition to 79% of proteins involved in branched-chain amino acid (BCCA) metabolism (15 of 19 proteins), 65% of proteins in the citric acid cycle (15 of 23 proteins), and 80% of proteins involved in ketone body metabolism (4 of 5 proteins) were acetylated. There was also a significant enrichment for proteins involved in oxidative phosphorylation and pyruvate metabolism, demonstrating specific mitochondrial pathways in acetyl-CoA production and utilization are widely acetylated.

Label-Free Quantitation of acK Peptides in WT and SIRT3$^{-/-}$ Mice. To identify true substrates of SIRT3 among all acetylated proteins and sites, we compared the relative level of acK peptide abundances between WT and KO mice using MS1 Filtering label-free quantitation. Although multiple peptides may be generated for a specific acK residue and targeted for quantitation, representative high-confidence peptides were selected based on having a tryptic cleavage at arginine or a nonacetylated lysine and lacking any secondary modifications. Once selected, the charge state with the highest signal intensity was used for quantitation, as secondary charge states, whereas generally in agreement (Dataset S3), had lower signal to noise and did not improve the overall statistics. Ion intensity measurements were normalized to a synthetic peptide standard, which had a coefficient of variation of 26%, indicating high reproducibility across samples. Of the 2,187 acK sites identified, quantitative data were obtained on 2,087 sites (Fig. 3*A*; Fig S1; Dataset S4). We found that acetylation at 283 sites present in 136 proteins increased more than twofold ($P \leq 0.01$) in KO mice at an FDR of 0.04, whereas only 11 acK peptides showed at least a twofold decrease. To control for possible changes in protein abundance in the SIRT3 KO mice that could contribute to altered levels of acK peptides, we also compared the levels of unmodified peptides from 350 mitochondrial proteins in nonenriched protein fractions (Fig S2; Dataset S5). The vast majority of proteins remained unchanged, suggesting that the absence of SIRT3 in the KO animals did not result in large compensatory changes in protein expression. Therefore, changes in the levels of acK peptides between the WT and KO mice observed after affinity enrichment

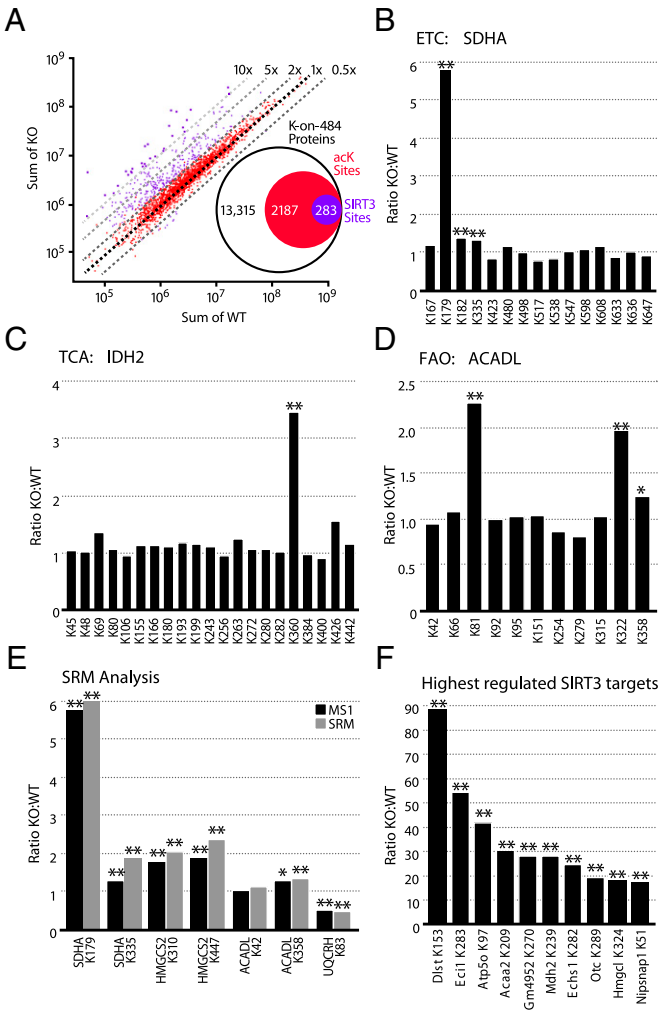

Fig. 3. Identification of SIRT3 substrates by label-free quantitation. (*A*) Scatter plot of the acK peptides quantitated by MS1 Filtering after normalization. Dashed lines indicate the fold change in intensity between WT and KO. Peptides with a significant ($P \leq 0.01$) at least twofold change are indicated in purple; all other peptides are in red. *Inset* summarizes the number of acK sites significantly changed in SIRT3$^{-/-}$ liver mitochondria from the total number of acK sites identified. Acetylation profiles of (*B*) succinate dehydrogenase subunit A (SDHA) from complex II in the ETC, (*C*) isocitrate dehydrogenase (IDH2) in the TCA cycle, and (*D*) long-chain specific acyl-CoA dehydrogenase (ACADL) in the fatty acid oxidation pathway. (*E*) Relative quantitation measurements resulting from SRM analysis of targeted acK sites using stable isotope dilution with synthetic peptide standards to the indicated proteins/acK sites. The most intense fragment ion was used for analysis and compared with MS1 Filtering results. (*F*) Largest fold changes (KO:WT) for individual acK sites. From left to right, dihydrolipoyllysine succinyltransferase (DLST), enoyl-CoA isomerase (ECI1), ATP synthase subunit O (ATP5O), 3-ketoacyl-CoA thiolase (ACAA2), Glycine *N*-acyltransferase-like protein (GM4952), malate dehydrogenase (MDH2), enoyl-CoA hydratase (ECHS1), ornithine carbamoyltransferase (OTC), hydroxymethylglutaryl-CoA lyase (HMGCL), and NipSnap homolog 1 (NIPSNAP1). Two-tailed Student *t* test (*$P \leq 0.05$, **$P \leq 0.01$); $n = 5$ for WT and KO with two injection replicates per sample.

can be almost exclusively attributed to alterations in acetylation levels at specific lysines.

Because there have been limited reports of substrates and sites of SIRT3 regulation, we examined our data against that previously reported for succinate dehydrogenase A (SDHA), IDH2, and ACADL. We quantified 21 acK sites in the succinate dehydrogenase complex, a four-subunit enzyme responsible for oxidizing succinate to fumarate and transferring electrons to ubiquinone. No change in acK levels of subunit B was detected (Dataset S4). However, acetylation at K179 on subunit A (SDHA) showed a robust increase in SIRT3$^{-/-}$ mice (Fig. 3*B*). The other 14 sites on SDHA were unchanged, indicating increased acetylation at K179 was specific for SIRT3 and not due to altered protein expression. These sites confirm our previous results for SDHA in SIRT3$^{-/-}$ mice from skeletal muscle mitochondria (26). In addition, we monitored 21 sites on the tricarboxylic acid (TCA) enzyme IDH2 and 11 sites on the FAO enzyme ACADL (14, 25) (Fig. 3 *C* and *D*). Of the 21 sites identified on IDH2, only K360 showed a significant increase in acetylation in SIRT3$^{-/-}$, whereas K322 on ACADL had increased acetylation.

Verification of MS1 Filtering Results by SRM/MS Analysis. To independently validate our label-free quantitative results, we developed selected reaction monitoring (SRM) assays for seven acK peptides identified in our study. SRM is sufficiently sensitive to quantify peptides in the low attomole range over a large dynamic range, and when coupled with stable isotope-labeled peptides, can measure absolute concentrations (29). Stable isotope-labeled synthetic peptides corresponding to seven acK peptides identified in our study were analyzed by SRM on a 5500 QTRAP after optimization of assay conditions. Stable isotope-labeled peptides were added to each of five WT and five KO acK-enriched samples for normalization and quantitation and analyzed in duplicate. SRM quantitative analysis shows nearly identical results to those generated using MS1 Filtering (Fig. 3*E*).

Pathway Analysis of SIRT3 Substrates Reveals Widespread Metabolic Targets with Multiple Sites. Site-specific changes measured by MS1 Filtering show the largest increase in acK levels for proteins from the TCA cycle [E2 component (DLST) of the α-ketoglutarate dehydrogenase complex and malate dehydrogenase (MDH2)], the electron transport chain [ATP synthase subunit O (ATP5O)], fatty acid oxidation (ECI1, ECHS1, ACAA2), the urea cycle [ornithine carbamoyltransferase (OTC)], and ketogenesis [hydroxmethylglutaryl-CoA lyase (HMGCL)] (Fig. 3*F*). To gain additional insight into these and other mitochondrial pathways regulated by SIRT3, we performed a pathway enrichment analysis (28) of all SIRT3 targets (Fig. 4*A*). We found that 71% of proteins involved in fatty acid oxidation (10 of 14 proteins), 43% of proteins in the TCA cycle (10 of 23 proteins), 53% of proteins involved in branched chain amino acid (BCAA) catabolism (10 of 19 proteins), and 80% of proteins involved in ketogenesis (4 of 5 proteins) have increased acK levels in KO mice. Protein expression levels measured in parallel by MS1 Filtering using up to six peptides from nonenriched mitochondrial digests showed minimal changes (Fig. S2; Dataset S5). For example the average KO:WT ratios of MDH2 and OTC were 1.09 and 1.08, respectively. Notably, of the proteins listed in Fig. 4*B*, only OTC has been previously reported as a substrate for SIRT3 (30, 31). Thus, SIRT3$^{-/-}$ mice show a profound increase in protein acetylation across mitochondrial pathways without significant alteration in protein expression.

Conservation of Lysine Acetylation Across Species. To gain insight into the evolutionary conservation of acK sites regulated by SIRT3, we generated a conservation index across vertebrate proteomes using AL2CO (32). Of the acK sites identified in mice, 87% of lysines were conserved in humans and 54% in *Danio rerio* (Fig. S3). Among lysines whose acetylation increased in SIRT3$^{-/-}$ mice, 85% were conserved in humans and 51% in *Danio rerio* (Fig. 4*B*). Many of the acK sites identified in mouse were mutated to arginine, which has a similar charge to lysine, or to glutamine, which has a similar structure to acetylated lysine and is often used as a mimetic. Notably, targets of SIRT3 are more likely to have mutated to arginine, whereas non–SIRT3-regulated sites are more likely to have mutated to glutamine (Fig. 4*C*), suggesting selective

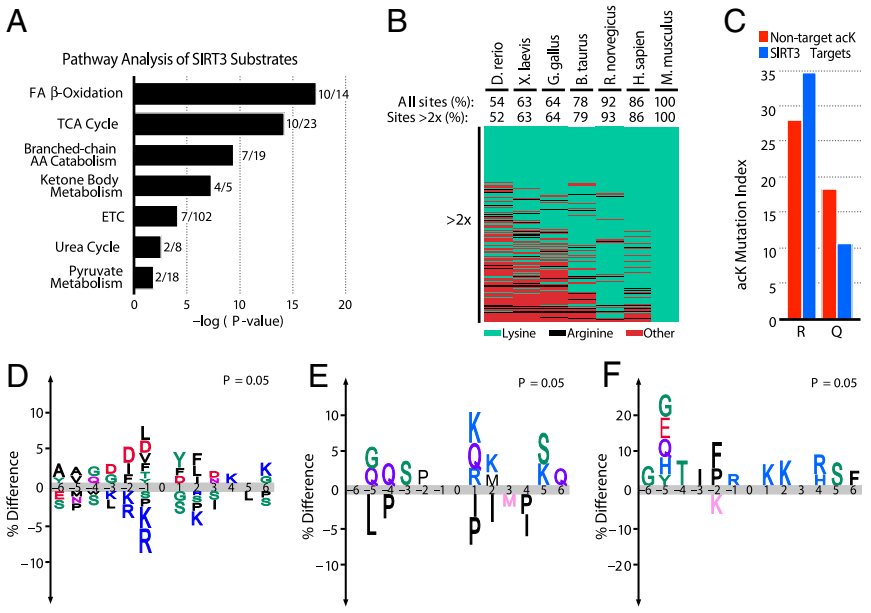

Fig. 4. Pathway and evolutionary analysis of acetylation sites and consensus motifs. (*A*) Pathway analysis of the mitochondrial acetylome altered in SIRT3$^{-/-}$ mice with the number of proteins identified per pathway. (*B*) Heat map depicting the conservation index of SIRT3 substrates (twofold increase) across seven vertebrate species with percent conservation calculated for all acK sites identified and SIRT3 substrates. Conservation index of all nonregulated sites is available in Fig. S3. (*C*) Percentage of acK residues identified in mouse mutated to arginine ($P = 0.01$) or glutamine ($P = 0.04$) across the seven species in Fig. 3*B* (P values calculated via χ^2 test). (*D*) Consensus sequence logos plot for acetylation sites ± six amino acids from the lysine of all acK sites identified, (*E*) from the identified lysine residues significantly increased in SIRT3$^{-/-}$ mice, and (*F*) for highly conserved acetylation sites significantly increased in SIRT3$^{-/-}$ mice.

pressure for maintaining a positively charged residue at sites regulated by SIRT3.

Sequence Motif Analysis of Mitochondrial- and SIRT3-Regulated Acetylation Sites. To determine whether there is a common sequence motif required for acetylation of mitochondrial proteins, we compared the amino acid sequences of all acetylated and nonacetylated sites using iceLogo (33) (Fig. 4*D*). A preference was observed for tyrosine at the +1 position and for aspartic acid at positions −1, −2, and −3, whereas positively charged residues are nearly excluded (2, 3, 34). SIRT3 substrates had no partiality to a negative charge preceding the acK site and preferred a positive charge at the +1 position (Fig. 4*E*). Interestingly, the sequence motif of highly conserved SIRT3 substrates from Fig. 4*B* showed a stronger preference for K at the +1 and +2 positions (Fig. 4*F*).

Discussion

Using a robust acK affinity workflow and label-free quantification, we identified 2,187 unique lysine acetylation sites across 483 proteins from isolated mitochondria, indicating that a majority of the matrix proteins are acetylated. Among acetylated proteins, 61% possess more than one site, suggesting the potential for multiple points of regulation. The absence of SIRT3 in liver leads to the selective hyperacetylation in the fasted mouse at 283 sites, representing 136 of the 483 acetylated mitochondrial proteins (Fig. 5). The largest fold changes in lysine acetylation were observed in key metabolic pathways including ATP synthase involved in oxidative phosphorylation, ECHS1 involved in fatty acid oxidation, OTC in the urea cycle, HMGCL involved in ketogenesis, and MDH2 from the TCA cycle. Last, we demonstrated that changes in acetylation levels were not due to altered protein expression, because quantitative analysis on 350 proteins from total mitochondrial protein hydrolysates was predominantly unchanged in KO mice.

Although acetylation is nearly ubiquitous among mitochondrial proteins, it is not evenly distributed. The pathways involved most directly in production and utilization of acetyl-CoA are heavily acetylated. These pathways are required for maintenance of glucose-poor fasting metabolism: fatty acid oxidation for acetyl CoA production; ketone body synthesis for distribution to other tissues; TCA cycle and oxidative phosphorylation for generation of ATP from acetyl CoA; amino acid catabolism for generation of TCA cycle intermediates and acetyl CoA; and urea cycle to metabolize nitrogen released by amino acid catabolism. The same pathways are abundant in SIRT3 targets as well, showing how SIRT3 may be a central regulator of mitochondrial adaptation to a fasting metabolic state. Many of these pathways were previously identified as containing a SIRT3 target, but our data show that regulation by SIRT3 is far more comprehensive; for example, every complex in the TCA cycle contains at least one SIRT3 target, as does every enzymatic step leading from fatty acids to the ketone body β-hydroxybutyrate (Fig. 5).

We identified three SIRT3-regulated sites on complex I components including NDUFA9 at K370. Previously, NDUFA9 was reported (18) as a SIRT3-interacting protein whose acetylation may reduce activity and decrease basal ATP levels. Additional SIRT3-regulated sites were identified on complex II at K179, one site on complex IV, and four sites on several components of ATP synthase. In the TCA cycle, both the α-ketoglutarate complex (KGDHC) and MDH2 had a ≥20-fold increase in acetylation levels at K153 and K239, respectively. The fact that KGDHC is sensitive to inhibition by oxidative stress (35) and implicated in the pathophysiology of neurodegeneration suggests that acetylation may be a key regulator of these processes (36). Although succinyl CoA synthetase did not have as dramatic an increase in acetylation, this TCA cycle enzyme had five sites with a greater than twofold increase. Interestingly, 40% of SIRT3 target proteins (54 of 136) are regulated at multiple sites, indicating the potential for differential or concerted regulation during fasting. Finally, we observed increased acetylation at 1 of 21 sites on IDH2 (K360). Taken together, our data identify several unique SIRT3-regulated components within the TCA cycle and oxidative phosphorylation pathways.

Proteins involved in fatty acid metabolism also featured prominently. For example, 10 of 14 proteins in the fatty acid oxidation pathway are hyperacetylated at 34 sites in KO mice (Fig. 5; Dataset S4). The most widely regulated SIRT3 substrate was the α-subunit (HADHA) of the trifunctional protein (TFP) complex. HADHA catalyzes two reactions in long-chain acyl-CoA oxidation, and its deficiency leads to hepatic steatosis and sudden death (37). Sixteen of 37 sites of acK on HADHA were significantly increased in SIRT3$^{-/-}$ with no change in protein expression levels, suggesting fine tuning of its regulation through multiple sites of acetylation. ACADL is upstream of TFP and catalyzes the initial step in the breakdown of long-chain acyl-CoAs. Of the proteins

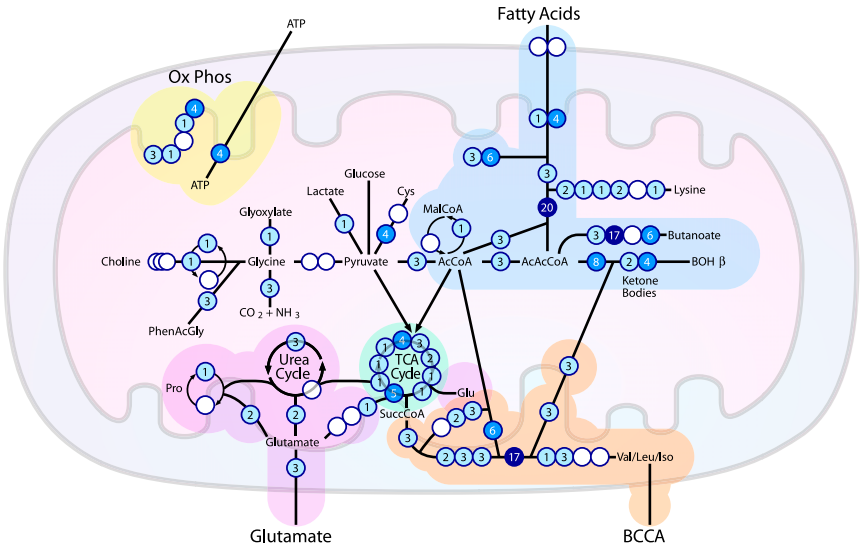

Fig. 5. Schematic depicting the primary SIRT3 regulated metabolic pathways within mitochondria including oxidative phosphorylation (Ox Phos), fatty acid oxidation, ketogenesis, branched chain amino acid catabolism (BCCA), the TCA cycle, and the urea cycle. Circles represent constituent proteins or protein complexes within each pathway with the number of SIRT3 regulatory sites indicated. Abbreviations include Acetyl-CoA (AcCoA), acetoacetyl-CoA (AcAcCoA), β-hydroxybutyrate (BOHβ), succinyl-CoA (SuccCoA), malonyl-CoA (MalCoA), ammonia (NH_3), carbon dioxide (CO_2), glutamate (Glu), proline (Pro), valine (Val), leucine (Leu), isoleucine (Iso), cysteine (Cys), adenosine triphosphate (ATP), and phenylacetylglycine (PhenAcGly).

involved in fatty acid oxidation, only ACADL was previously reported as a substrate for SIRT3 through regulation at K42 (14). MS1 Filtering showed a 2.1-fold increase in acetylation on ACADL at K322 but no change at K42, which was confirmed by SRM-MS analysis. Taken together, our data suggest SIRT3 regulates acyl-CoA oxidation at multiple points in the pathway for long- and short-chain acyl-CoAs, as well as saturated and unsaturated fatty acids. Indeed, these data support a previous study (14) showing inhibition of the fatty acid oxidation pathway through elevated long-chain acylcarnitine accumulation in liver and plasma and development of hepatic steatosis in SIRT3$^{-/-}$ mice.

The majority of proteins involved in ketone body production had elevated levels of acetylation in SIRT3$^{-/-}$ animals. Mice deficient for SIRT3 were previously shown to have decreased ketone body production and hyperacetylation of HMGCS2 (19). We observed only modest increases in acetylation at K310, K447, and K473 for HMGCS2 in contrast to a previous report (19) that observed robust increases at K46, K83, and K333. To address this discrepancy in HMGCS2, SRM-MS assays were carried out using synthetic peptides that confirmed our MS1 Filtering results. Elevated levels of SIRT3 in the liver during the fasted state may lead to activation of ketogenic enzymes by SIRT3 to meet energetic demands in other tissues.

The BCAA pathway responds to changes in dietary flux when other nutrient sources become limited to maintain energy homeostasis. It is not surprising, therefore, that the acetylation of several proteins from the BCAA pathway was found to increase significantly in the SIRT3$^{-/-}$ mouse. Methylglutaconyl-CoA hydratase (AUH), which catalyzes the breakdown of 3-methylglutaconyl-CoA to 3-hydroxy-3-methylglutaryl-CoA, showed moderate to robust increases in acetylation levels at K47, K119, and K304. Likewise, the E2 subunit of the branched-chain α-ketoacid dehydrogenase complex, whose deficiency causes maple syrup urine disease, was also hyperacetylated at three sites including K82 within the lipoyl binding domain, suggesting a likely regulation by SIRT3 of the activity of this protein as well and multiple regulated steps in this pathway. The increase in acetylation among enzymes of the BCAA pathway is consistent with the previously reported small increase in BCAAs in the SIRT3 mouse liver, assuming acetylation leads to a decrease in enzymatic activity (14).

SIRT3 is not simply a global deacetylase, because some proteins such as CPS1 and GDH are widely acetylated yet have few SIRT3-regulated sites. CPS1, which catalyzes the synthesis of carbamoyl phosphate from glutamine in the urea cycle, was hyperacetylated at only 2 of 70 acK sites in the KO mouse. Such a large difference suggests that SIRT3 is selective, even for proteins that are extensively acetylated. Conversely, some proteins such as Lon peptidase and the Ts translation elongation factor have a very small number of acetylation sites, yet the majority are SIRT3 regulated. In contrast, HADHA was found to be both highly acetylated (37 sites) and highly regulated, with almost half (16 sites) identified as SIRT3 targets. Thus, SIRT3 appears to target specific lysines among highly acetylated proteins involved in adaptation to fasting metabolism while also having some apparently idiosyncratic targets that may be related more generally to mitochondrial maintenance.

We investigated the conservation of SIRT3-regulated sites across several vertebrate proteomes. Surprisingly, sites regulated by SIRT3 were no more highly conserved than acK sites unchanged in the KO mouse, nor was there a significant conservation of SIRT3 regulated sites in a given pathway. However, there was a noticeable preference towards maintaining a positively charged amino acid at SIRT3-regulated acK sites. Although highly conserved sites provided a greater understanding of the SIRT3-regulated acK motif, it did not dramatically improve our ability to predict a SIRT3 consensus sequence. Thus, SIRT3 may be promiscuous in its primary sequence selectivity, and site-specific regulation may be due to other factors such as solvent accessibility or tertiary structure. In addition, the significance of the non–SIRT3-regulated acetylation sites remains unclear given the absence of alternative mitochondrial deacetylases. Combined with the lack of a clearly identified mitochondrial acetyltransferase(s), acetylation may be derived from nonenzymatic processes due to the high pH (~7.9) and high concentration of AcCoA (~5 mM) in this organelle, although no differences were reported in AcCoA levels in the liver of SIRT3 KO mice (38).

Although our experimental approach measures the relative level of acetylation at a given site in the presence and absence of SIRT3, it does not use absolute criteria in identifying (or excluding) a SIRT3-regulated site nor does it use information on stoichiometry. Our threshold of at least twofold ($P \leq 0.01$) for a SIRT3-regulated site was chosen primarily to have a low FDR (<0.05), thus ensuring the integrity of the proteome-wide data set. The lack of stoichiometry information presents different challenges. For example, sites that are ≥50% acetylated under basal conditions would not achieve a twofold increase in acetylation. Alternatively, sites at very low levels of acetylation present a problem of biological relevance. However, proteomic experiments carried out without enrichment identify very few acetylation sites, consistent with low to moderate levels of lysine acetylation. Nonetheless, defining the precise stoichiometry of acetylation

at individual sites is clearly needed to answer these questions, a process that is currently limited by a lack of robust methodology despite some limited success reported for histones (39).

Although SIRT3 is the predominant mitochondrial deacetylase, recent work has shown SIRT5 to have both lysine desuccinylase and demalonylase activities (10, 11). Proteomic studies identified lysine malonylation of MDH2, GDH, and ADP/ATP translocase 2 that overlap with acK sites identified here (10, 11). Similarly, lysine succinylation was identified on GDH, MDH2, citrate synthase, and HMGCS2 at SIRT3-regulated acK sites (10). Therefore, cross-talk among the different types of lysine acylation in mitochondria may provide complex avenues of regulation similar to that of histone modifications (40).

Conclusion

In summary, we combined a unique label-free quantitative proteomic approach with efficient enrichment of lysine acetylated peptides to identify the SIRT3-regulated acetylome in liver mitochondria. Using a SIRT3$^{-/-}$ mouse model, we identified 283 sites among 136 proteins as SIRT3-specific substrates. Moreover, we independently validated a subset of these peptides using SRM-MS, demonstrating the accuracy of our results. Our data showed broad regulation of multiple proteins and sites across several key mitochondrial pathways involved in nutrient signaling and energy homeostasis. Proteins involved in regulating fatty acid oxidation were particularly targeted by SIRT3 and indicate the potential for regulation during changes in nutrient availability. Surprisingly, a large disparity can exist between the extent of lysine acetylation in a given protein and those sites that are regulated by SIRT3, as demonstrated by CPS1 and HADHA. However, the majority of the 2,187 acetylated sites we identified did not appear to be regulated by SIRT3, suggesting many of these sites may have little or no functional consequence or simply failed to meet our rigorous inclusion threshold. Although our study was designed to be comprehensive, technical and sampling limitations may have limited its completeness. Nonetheless, our large-scale inventory of acetylated proteins and sites in the liver mitochondria significantly expands our understanding of how SIRT3 may regulate mitochondrial function and represents an important step toward elucidating the role of SIRT3 in the liver and other tissues. Future studies will need to address the stoichiometry of acetylation at different sites, possible competition between different acyl modifications, and the functional role of acetylation on protein function under normal and pathological conditions.

Materials and Methods

The experimental workflow of acK peptide enrichment from mitochondria and their MS analysis and quantitation by MS1 Filtering are briefly outlined in Fig. 1 and in *Results*. Additional information on organelle enrichment, antibodies, chemicals, protein preparation, immunoprecipitation of acK peptides, determination of conservation, experimental MS parameters, label-free quantitation by MS1 Filtering, and SRM are provided in *SI Materials and Methods* and Dataset S6. All acK peptide spectra are available for viewing online at https://skyline.gs.washington.edu:9443/labkey/project/Gibson/Gibson_Reviewer/begin.view?.

ACKNOWLEDGMENTS. This work was supported by National Institutes of Health Grants T32AG000266 (to M.J.R.), PL1 AG032118 (to B.W.G.), and R24 DK085610 (to E.V.). This work was also supported in part by the Shared Instrumentation Grant S10 RR024615 (to B.W.G.) and the generous access of a TripleTOF 5600 by AB SCIEX at the Buck Institute.

1. Glozak MA, Sengupta N, Zhang X, Seto E (2005) Acetylation and deacetylation of non-histone proteins. *Gene* 363:15–23.
2. Kim SC, et al. (2006) Substrate and functional diversity of lysine acetylation revealed by a proteomics survey. *Mol Cell* 23(4):607–618.
3. Choudhary C, et al. (2009) Lysine acetylation targets protein complexes and co-regulates major cellular functions. *Science* 325(5942):834–840.
4. DiMauro S, Schon EA (2003) Mitochondrial respiratory-chain diseases. *N Engl J Med* 348(26):2656–2668.
5. Beal MF (2005) Mitochondria take center stage in aging and neurodegeneration. *Ann Neurol* 58(4):495–505.
6. Schwer B, Verdin E (2008) Conserved metabolic regulatory functions of sirtuins. *Cell Metab* 7(2):104–112.
7. Schwer B, North BJ, Frye RA, Ott M, Verdin E (2002) The human silent information regulator (Sir)2 homologue hSIRT3 is a mitochondrial nicotinamide adenine dinucleotide-dependent deacetylase. *J Cell Biol* 158(4):647–657.
8. Michishita E, Park JY, Burneskis JM, Barrett JC, Horikawa I (2005) Evolutionarily conserved and nonconserved cellular localizations and functions of human SIRT proteins. *Mol Biol Cell* 16(10):4623–4635.
9. Lombard DB, et al. (2007) Mammalian Sir2 homolog SIRT3 regulates global mitochondrial lysine acetylation. *Mol Cell Biol* 27(24):8807–8814.
10. Du J, et al. (2011) Sirt5 is a NAD-dependent protein lysine demalonylase and desuccinylase. *Science* 334(6057):806–809.
11. Peng C, et al. (2011) The first identification of lysine malonylation substrates and its regulatory enzyme. *Mol Cell Proteomics* 10(12):M111012658.
12. Haigis MC, et al. (2006) SIRT4 inhibits glutamate dehydrogenase and opposes the effects of calorie restriction in pancreatic beta cells. *Cell* 126(5):941–954.
13. Schwer B, et al. (2009) Calorie restriction alters mitochondrial protein acetylation. *Aging Cell* 8(5):604–606.
14. Hirschey MD, et al. (2010) SIRT3 regulates mitochondrial fatty-acid oxidation by reversible enzyme deacetylation. *Nature* 464(7285):121–125.
15. Jing E, et al. (2011) Sirtuin-3 (Sirt3) regulates skeletal muscle metabolism and insulin signaling via altered mitochondrial oxidation and reactive oxygen species production. *Proc Natl Acad Sci USA* 108(35):14608–14613.
16. Cimen H, et al. (2010) Regulation of succinate dehydrogenase activity by SIRT3 in mammalian mitochondria. *Biochemistry* 49(2):304–311.
17. Finley LW, et al. (2011) Succinate dehydrogenase is a direct target of sirtuin 3 deacetylase activity. *PLoS ONE* 6(8):e23295.
18. Ahn BH, et al. (2008) A role for the mitochondrial deacetylase Sirt3 in regulating energy homeostasis. *Proc Natl Acad Sci USA* 105(38):14447–14452.
19. Shimazu T, et al. (2010) SIRT3 deacetylates mitochondrial 3-hydroxy-3-methylglutaryl CoA synthase 2 and regulates ketone body production. *Cell Metab* 12(6):654–661.
20. Chen Y, et al. (2011) Tumour suppressor SIRT3 deacetylates and activates manganese superoxide dismutase to scavenge ROS. *EMBO Rep* 12(6):534–541.
21. Qiu X, Brown K, Hirschey MD, Verdin E, Chen D (2010) Calorie restriction reduces oxidative stress by SIRT3-mediated SOD2 activation. *Cell Metab* 12(6):662–667.
22. Tao R, et al. (2010) Sirt3-mediated deacetylation of evolutionarily conserved lysine 122 regulates MnSOD activity in response to stress. *Mol Cell* 40(6):893–904.
23. Bell EL, Emerling BM, Ricoult SJ, Guarente L (2011) SirT3 suppresses hypoxia inducible factor 1α and tumor growth by inhibiting mitochondrial ROS production. *Oncogene* 30(26):2986–2996.
24. Finley LW, et al. (2011) SIRT3 opposes reprogramming of cancer cell metabolism through HIF1α destabilization. *Cancer Cell* 19(3):416–428.
25. Someya S, et al. (2010) Sirt3 mediates reduction of oxidative damage and prevention of age-related hearing loss under caloric restriction. *Cell* 143(5):802–812.
26. Schilling B, et al. (2012) Platform-independent and label-free quantitation of proteomic data using MS1 extracted ion chromatograms in skyline: Application to protein acetylation and phosphorylation. *Mol Cell Proteomics* 11(5):202–214.
27. Zhang H, *et al.* (2011) Methods for peptide and protein quantitation by liquid chromatography-multiple reaction monitoring mass spectrometry. *Mol Cell Proteomics* 10(6):M110006593.
28. Croft D, et al. (2011) Reactome: a database of reactions, pathways and biological processes. *Nucleic Acids Res* 39(Database issue):D691–D697.
29. Gerber SA, Rush J, Stemman O, Kirschner MW, Gygi SP (2003) Absolute quantification of proteins and phosphoproteins from cell lysates by tandem MS. *Proc Natl Acad Sci USA* 100(12):6940–6945.
30. Hallows WC, et al. (2011) Sirt3 promotes the urea cycle and fatty acid oxidation during dietary restriction. *Mol Cell* 41(2):139–149.
31. Yu W, et al. (2009) Lysine 88 acetylation negatively regulates ornithine carbamoyltransferase activity in response to nutrient signals. *J Biol Chem* 284(20):13669–13675.
32. Pei J, Grishin NV (2001) AL2CO: Calculation of positional conservation in a protein sequence alignment. *Bioinformatics* 17(8):700–712.
33. Colaert N, Helsens K, Martens L, Vandekerckhove J, Gevaert K (2009) Improved visualization of protein consensus sequences by iceLogo. *Nat Methods* 6(11):786–787.
34. Lundby A, et al. (2012) Proteomic analysis of lysine acetylation sites in rat tissues reveals organ specificity and subcellular patterns. *Cell Rep* 2(2):419–431.
35. Tretter L, Adam-Vizi V (2000) Inhibition of Krebs cycle enzymes by hydrogen peroxide: A key role of [alpha]-ketoglutarate dehydrogenase in limiting NADH production under oxidative stress. *J Neurosci* 20(24):8972–8979.
36. Gibson GE, Blass JP, Beal MF, Bunik V (2005) The alpha-ketoglutarate-dehydrogenase complex: A mediator between mitochondria and oxidative stress in neurodegeneration. *Mol Neurobiol* 31(1-3):43–63.
37. Ibdah JA, et al. (2001) Lack of mitochondrial trifunctional protein in mice causes neonatal hypoglycemia and sudden death. *J Clin Invest* 107(11):1403–1409.
38. Hirschey MD, et al. (2011) SIRT3 deficiency and mitochondrial protein hyperacetylation accelerate the development of the metabolic syndrome. *Mol Cell* 44(2):177–190.
39. Smith CM, et al. (2003) Mass spectrometric quantification of acetylation at specific lysines within the amino-terminal tail of histone H4. *Anal Biochem* 316(1):23–33.
40. Latham JA, Dent SY (2007) Cross-regulation of histone modifications. *Nat Struct Mol Biol* 14(11):1017–1024.

Supporting Information

Rardin et al. 10.1073/pnas.1302961110

SI Methods and Materials

Materials. HPLC solvents including acetonitrile and water were obtained from Burdick & Jackson. Reagents for protein chemistry including iodoacetamide, DTT, ammonium bicarbonate, formic acid, trifluoroacetic acid, trichostatin A, dodecyl-maltoside, urea, nicotinamide, and BSA were purchased from Sigma Aldrich. Acetylated synthetic peptides containing stable isotope labeled lysine or arginine residues ($^{13}C_6{}^{15}N_2$-Lys and $^{13}C_6{}^{15}N_4$-Arg, respectively) were obtained from Thermo Fisher Scientific at >95% purity. Tris(2-carboxyethyl)phosphine (TCEP) was purchased from Thermo, and HLB Oasis SPE cartridges were purchased from Waters. Protein G agarose was obtained from Pierce, and proteomics grade trypsin was from Promega. Anti–glutamate dehydrogenase antibody was purchased from Rockland. Trypsin-predigested β-galactosidase (a quality control standard) was purchased from AB SCIEX.

MS and Chromatographic Parameters. All samples used for MS1 Filtering experiments were analyzed by reverse-phase liquid chromatography-electrospray ionization-MS/MS using an Eksigent Ultra Plus nano-LC 2D HPLC system connected to a quadrupole time-of-flight TripleTOF 5600 mass spectrometer (AB SCIEX) in direct injection mode. The autosampler was operated in full injection mode overfilling a 1-μL loop with 3 μL analyte for optimal sample delivery reproducibility. Briefly, after injection, peptide mixtures were transferred onto the analytical C18-nano-capillary LC column (C18 Acclaim PepMap100, 75-μm ID × 15 cm, 3-μm particle size, 100-Å pore size; Dionex) and eluted at a flow rate of 300 nL/min using the following gradient: at 3% (vol/vol) solvent B in A (from 0 to 13 min), 3–7% (vol/vol) solvent B in A (from 13 to 16 min), 7–25% (vol/vol) solvent B in A (from 16 to 48 min), 25–40% (vol/vol) solvent B in A (from 48 to 65 min), 40–90% (vol/vol) solvent B in A (from 65 to 75 min), and at 90% (vol/vol) solvent B in A (from 75 to 85 min), with a total run time of 120 min including mobile phase equilibration. Solvents were prepared as follows: mobile phase A, 2% acetonitrile/98% of 0.1% formic acid (vol/vol) in water; mobile phase B, 98% acetonitrile/2% of 0.1% formic acid (vol/vol) in water. Mass spectra and tandem mass spectra were recorded in positive-ion and high-sensitivity mode with a resolution of ∼35,000 full-width half-maximum in MS1 and 15,000 in MS2. The nanospray needle voltage was typically 2,400 V in HPLC-MS mode. After acquisition of approximately five to six samples, TOF MS spectra and TOF MS/MS spectra were automatically calibrated during dynamic LC-MS and MS/MS autocalibration acquisitions injecting 25 fmol β-galactosidase. For collision-induced dissociation tandem MS (CID-MS/MS), the mass window for precursor ion selection of the quadrupole mass analyzer was set to ±1 *m/z*. The precursor ions were fragmented in a collision cell using nitrogen as the collision gas. Advanced information-dependent acquisition (IDA) was used for MS/MS collection on the TripleTOF 5600 to obtain MS/MS spectra for the 20 most abundant parent ions following each survey MS1 scan (allowing typically for 50 ms acquisition time per each MS/MS, which for some experiments was increased to 75 ms). Dynamic exclusion features were based on value M not *m/z* and were set to an exclusion mass width of 50 mDa and an exclusion duration of 15–20 s. MS/MS spectra for all identified peptides may be viewed using Panorama (1) at the following location: https://skyline.gs.washington.edu:9443/labkey/project/Gibson/Gibson_Reviewer/begin.view?; raw data files are available for download at the following location: ftp://sftp.buckinstitute.org/Gibson.

For selected reaction monitoring (SRM), samples were analyzed by nano-LC-SRM/MS on a 5500 QTRAP hybrid triple quadrupole/linear ion trap mass spectrometer (AB SCIEX). Chromatography was performed on a NanoLC-Ultra 2D LC system (Eksigent) with buffer A [0.1% (vol/vol) formic acid] and buffer B (90% acetonitrile in 0.1% formic acid). Digests were separated on a 15-cm-long, 75-μm reversed phase C18 column (3 μm, 120Å; Eksigent) in a cHiPLC nanoflex chip configuration at a flow rate 300 nL/min. Gradient was 3% B from 0 to 5 min, increased to 15% B over 3 min, and increased to 35% B over the next 34 min. Peptides were ionized using a PicoTip emitter (20 μm, 10-μm tip; New Objective). Data acquisition was performed using Analyst 1.5.1 (AB SCIEX) with an ion spray voltage of 2,300 V, curtain gas of 20 psi, nebulizer gas of 15 psi, and interface heater temperature of 150 °C.

The transitions, dwell times, and collision energy are listed in Dataset S6. Four transitions were assayed per peptide. The declustering potential and collision energy for each transitions were optimized with using stable isotope-labeled synthetic peptides, labeled at the C terminus with either $^{13}C_6{}^{15}N_2$-Lys or $^{13}C_6{}^{15}N_4$-Arg. Retention time scheduling was also used with a retention time window of 240 s and a target scan time of 1.5 s. A value of 40 was used as the collision cell exit potential for all transitions. Selected reaction monitoring (SRM) transitions were acquired at unit resolution both in the first and third quadrupoles (Q1 and Q3). Standard curves were performed in triplicate by spiking in the stable isotope-labeled peptide to determine the linear range, limit of detection (LOD), and limit of quantitation (LOQ) in a background matrix of 250 ng of protein (2). Skyline postacquisition software was used to process all SRM data (3). Samples were analyzed in duplicate with 25 fmol of each heavy peptide spiked in. Each transition was individually integrated to generate peak areas, and the peak area of the most intense area was used for analysis.

Bioinformatic Database Searches. Mass spectral data sets were analyzed and searched using Mascot server version 2.3.02 (Matrix Sciences) and ProteinPilot (revision 148085; AB SCIEX 4.0) using the Paragon algorithm (4.0.0.0, 148083). All data files were searched using the SwissProt 2011_08 database with a total of 531,473 sequences but were restricted to *Mus musculus* (16,441 protein sequences). Search parameters in Mascot for acetylated peptides were as follows: trypsin digestion with four missed cleavages to account for the inability of trypsin to cleave at acetylated lysine residues. Trypsin specificity was set to C-terminal cleavage at lysine and arginine. Variable modifications included lysine acetylation, methionine oxidation, conversion of glutamine to pyroglutamic acid, and deamidation of asparagine. Carbamidomethyl cysteine was set as a fixed modification. Precursor ion and fragment ion mass tolerances were set to 20 ppm and 0.2 Da, respectively. Peptides with an expectation value <1% false discovery rate (FDR) were chosen for further data processing.

The following sample parameters were used in Protein Pilot: trypsin digestion, cysteine alkylation set to iodoacetamide, urea denaturation, and acetylation emphasis. Processing parameters were set to "Biological modification," and a thorough ID search effort was used. A local FDR of 1% was chosen using the Protein Pilot FDR analysis tool (PSPEP) algorithm (4). All mass spectral details for acetylated peptides are available in Dataset S1. For non-acetylated peptide searches, the acetylation emphasis was not used, and a peptide confidence value of 95 was chosen; mass spectral details for nonenriched peptides are available in Dataset S5.

Skyline MS1 Filtering Tool Algorithm and Data Analysis. Skyline is an open source software project and can be freely installed. Additional details and tutorials for creating spectral libraries and MS1 Filtering can be viewed on the Skyline website (http://proteome.gs.washington.edu/software/skyline). Spectral libraries were generated in Skyline using the BiblioSpec algorithm (5) from database searches of the raw data files as previously described (6). Raw files were directly imported into Skyline in their native file format, which Skyline achieves using the ProteoWizard data access library (7). After data import, graphical displays of chromatographic traces for the top three isotopic peaks were manually inspected for proper peak picking of MS1 filtered peptides. All quantitations performed in this study were done on the peptide level, using a peptide centric approach. Only the most abundant isotope for each peptide was used for quantitation. Following data extraction, peptide areas were normalized to the spiked in acetyllysine peptide standard (m/z 626.8604^{++}; LVSSVSDLPacKR, where acetylated lysine (acK) is *N*-acetyllysine and R = $^{13}C_6{}^{15}N_4$-Arg) and then multiplied by a normalization factor 1e^7 to ensure all values were >1. The normalized peptide area was then averaged across all WT or SIRT3$^{-/-}$ acquisitions, and a ratio was generated (KO:WT). *P* values were calculated using a two-tailed, unpaired Student *t* test. All details for peptide quantitation using MS1 Filtering are provided in Datasets S3, S4, and S5. The FDR for the SIRT3 target proteins was calculated using the Benjamini–Hochberg procedure.

Conservation Index of Lysine Acetylation Sites. For each mouse protein containing one or more acetylation sites, the full sequence was downloaded from UniProt and then aligned to the nr database by blastpgp (BLAST suite 2.2.18) (8). To construct a high-quality multiple sequence alignment, we applied two criteria to all hits in each alignment sequentially: (*i*) sequence identity between 30% and 94% to the quest mouse protein; and (*ii*) >10 such hits could be found. We then generated a multiple sequence alignment on selected hits and original mouse protein by CLUSTALW (2.0.12) using default parameter settings (9). Finally, we used AL2CO on the output of CLUSTALW to compute conservation index on each aligned column and extracted corresponding values for all annotated acetylation sites (10).

Sample Preparation for Mouse Liver Mitochondrial Protein Lysate. Livers were extracted from five WT and five SIRT3$^{-/-}$ male mice at 17 wk of age following a 24-h fast in the presence of deacetylase inhibitors (10 mM nicotinamide and 0.5 μM trichostatin A). Mitochondria were isolated by differential centrifugation as described previously (11). Mitochondrial protein (1.05 mg/mouse) was denatured with 1% dodecyl-maltoside and 10 M urea per process replicate. Samples were then diluted 1:10, reduced with 4.5 mM TCEP (37 °C for 1 h), alkylated with 10 mM iodoacetamide (30 min at room temperature in the dark), and incubated overnight at 37 °C with sequencing grade trypsin added at a 1:50 enzyme:substrate ratio (wt/wt). Samples were then acidified with formic acid and desalted using HLB Oasis SPE cartridges. Samples were eluted, concentrated to near dryness by vacuum centrifugation, and resuspended in NET buffer (50 mM Tris-HCl, pH 8.0, 100 mM NaCl, 1 mM EDTA). Protein digest from each sample (50 μg) was desalted using C-18 zip-tips for total peptide analysis of samples by MS1 Filtering, whereas the remaining 1 mg was used for affinity purification of lysine-acetylated peptides.

Affinity Purification of Lysine-Acetylated Peptides. The polyclonal anti-acetyllysine antibodies (Cell Signaling 9441) were immobilized on protein G agarose beads (4 °C, 2 h) and combined with an equal amount of prewashed anti-acetyllysine agarose antibody conjugate (ImmuneChem ICP0380-100). Acetyllysine peptide standard (100 fmol; m/z 626.8604^{++}; LVSSVSDLPacKR) was added to the digested peptides from the above mitochondrial protein lysate and incubated overnight (4 °C) at a 1:25 antibody:peptide ratio (wt/wt). Beads were washed three times in NET buffer, and the peptides were eluted by washing three times in 1% trifluoroacetic acid/40% acetonitrile (vol/vol). Peptides are concentrated to near dryness by vacuum centrifugation and resuspended in equal amounts of 0.1% formic acid/1% acetonitrile. The acetyllysine peptide enrichments were subsequently desalted using C-18 zip-tips. After evaporation of organic solvents, samples were suspended in 0.1% formic acid/1% acetonitrile and analyzed by LC-MS/MS on the TripleTOF 5600. A solution-only "blank" was run in between sample acquisition to prevent carryover that would affect downstream quantitative analysis.

1. Sharma V, et al. (2012) Panorama: A private repository of targeted proteomics assays for Skyline. *Proceedings of the 60th ASMS Conference on Mass Spectrometry and Allied Topics*, American Society for Mass Spectrometry, May 20th-24th Vancouver, BC (American Society for Mass Spectrometry, Santa Fe, NM).
2. Shrivastava A, Gupta VB (2011) Methods for the determination of limit of detection and limit of quantitation of the analytical methods. *Chron Young Sci* 2(1): 21–25.
3. MacLean B, et al. (2010) Skyline: An open source document. for creating and analyzing targeted proteomics experiments. *Bioinformatics* 26(7):966–968.
4. Shilov IV, et al. (2007) The Paragon Algorithm, a next generation search engine that uses sequence temperature values and feature probabilities to identify peptides from tandem mass spectra. *Mol Cell Proteomics* 6(9):1638–1655.
5. Frewen B, MacCoss MJ (2007) Using BiblioSpec for creating and searching tandem MS peptide libraries. *Curr Protoc Bioinform*, pp 20:13.7.1-13.7.12.
6. Schilling B, et al. (2012) Platform-independent and label-free quantitation of proteomic data using MS1 extracted ion chromatograms in skyline: Application to protein acetylation and phosphorylation. *Mol Cell Proteomics* 11(5):202–214.
7. Kessner D, Chambers M, Burke R, Agus D, Mallick P (2008) ProteoWizard: open source software for rapid proteomics tools development. *Bioinformatics* 24(21):2534–2536.
8. Altschul SF, et al. (1997) Gapped BLAST and PSI-BLAST: A new generation of protein database search programs. *Nucleic Acids Res* 25(17):3389–3402.
9. Larkin MA, et al. (2007) Clustal W and Clustal X version 2.0. *Bioinformatics* 23(21): 2947–2948.
10. Pei J, Grishin NV (2001) AL2CO: calculation of positional conservation in a protein sequence alignment. *Bioinformatics* 17(8):700–712.
11. Rardin MJ, Wiley SE, Naviaux RK, Murphy AN, Dixon JE (2009) Monitoring phosphorylation of the pyruvate dehydrogenase complex. *Anal Biochem* 389(2):157–164.

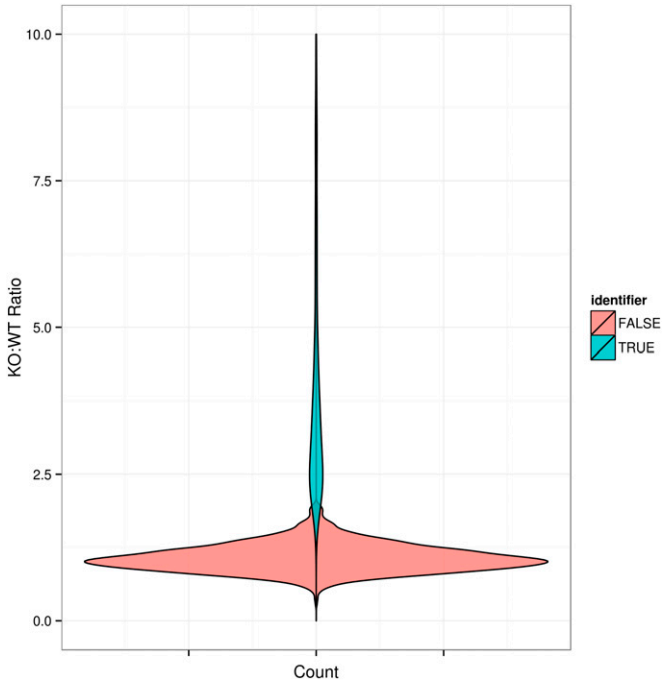

Fig. S1. Volcano plot showing the distribution of acetylation sites quantitated with the majority of sites having a ratio (KO:WT) near 1. Peptides with greater than a twofold change and $P < 0.01$ were considered "true" SIRT3 targets. Two-tailed Student *t* test (*$P < 0.05$, **$P < 0.01$); $n = 5$ for WT and KO with two injection replicates per sample.

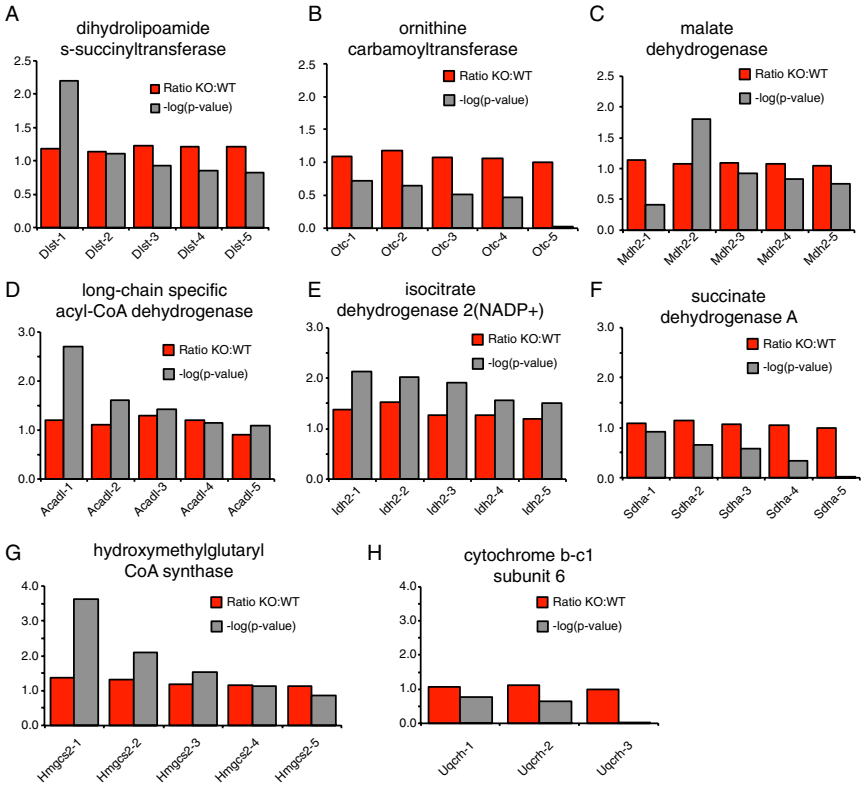

Fig. S2. Quantitation of peptides from mitochondrial digests for determining protein expression levels. Relative ratio (KO:WT) shown in red bars of five separate peptides quantitated by MS1 Filtering from (*A*) dihydrolipoamide s-succinyltransferase (DLST), (*B*) ornithine carbamoyltransferase (OTC), (*C*) malate dehydrogenase (MDH2), (*D*) long-chain specific acyl-CoA dehydrogenase (ACADL), (*E*) isocitrate dehydgrogenase ($NADP^+$) (IDH2), (*F*) succinate dehydrogenase subunit A (SDHA), (*G*) hydroxmethylglutaryl-CoA synthase (HMGCS2), and (*H*) cytochrome *b*-c1 subunit 6 (UGCRH). Two-tailed Student *t* test [−log(*P* value)] shown in gray bars; $n = 5$ for WT and $SIRT3^{-/-}$(KO) with two injection replicates per sample.

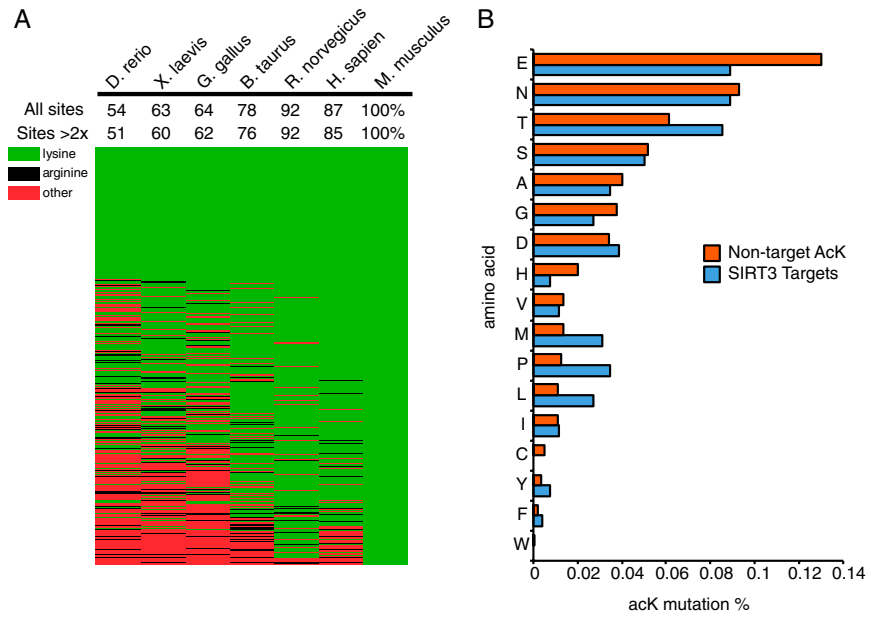

Fig. S3. Conservation of non-SIRT3 regulated acetylation sites. (*A*) Conservation index of acK sites identified in mouse across seven species that were not significantly increased in SIRT3$^{-/-}$ mice. Lysine residues are in green, arginine, which is the most similar amino acid in charge and structure to lysine, is in black, and all other amino acids are in red. (*B*) The percentage of acK sites identified in mouse that are mutated to other amino acids. Sites are distinguished based on whether they were up-regulated in SIRT3$^{-/-}$ animals.

Other Supporting Information Files

Dataset S1 (XLSX)
Dataset S2 (XLSX)
Dataset S3 (XLSX)
Dataset S4 (XLSX)
Dataset S5 (XLSX)
Dataset S6 (XLSX)